HHS Public Access

Author manuscript

Neuroimage. Author manuscript; available in PMC 2018 January 01.

Published in final edited form as:

Neuroimage. 2017 January 01; 144(Pt A): 164–173. doi:10.1016/j.neuroimage.2016.10.008.

Beta-band Activity and Connectivity in Sensorimotor and Parietal Cortex are Important for Accurate Motor Performance

Jae W. Chung[1,4], **Edward Ofori**[1,4], **Gaurav Misra**[1], **Christopher W. Hess**[2], and **David E. Vaillancourt**[1,2,3,*]

[1]Department of Applied Physiology and Kinesiology, University of Florida, Gainesville, FL, 32611, USA

[2]Department of Neurology, University of Florida, Gainesville, FL, 32610, USA

[3]Department of Biomedical Engineering, University of Florida, Gainesville, FL, 32611, USA

Abstract

Accurate motor performance may depend on the scaling of distinct oscillatory activity within the motor cortex and effective neural communication between the motor cortex and other brain areas. Oscillatory activity within the beta-band (13–30 Hz) has been suggested to provide distinct functional roles for attention and sensorimotor control, yet it remains unclear how beta-band and other oscillatory activity within and between cortical regions is coordinated to enhance motor performance. We explore this open issue by simultaneously measuring high-density cortical activity and elbow flexor and extensor neuromuscular activity during ballistic movements, and manipulating error using high and low visual gain across three target distances. Compared with low visual gain, high visual gain decreased movement errors at each distance. Group analyses in 3D source-space revealed increased theta-, alpha-, and beta-band desynchronization of the contralateral motor cortex and medial parietal cortex in high visual gain conditions and this corresponded to reduced movement error. Dynamic causal modeling was used to compute connectivity between motor cortex and parietal cortex. Analyses revealed that gain affected the directionally-specific connectivity across broadband frequencies from parietal to sensorimotor cortex but not from sensorimotor cortex to parietal cortex. These new findings provide support for the interpretation that broad-band oscillations in theta, alpha, and beta frequency bands within sensorimotor and parietal cortex coordinate to facilitate accurate upper limb movement.

[*]Corresponding author: David E. Vaillancourt Department of Applied Physiology and Kinesiology University of Florida PO Box 118205 vcourt@ufl.edu (o) +1 352 294 1770 (f) +1 352 392 5262.

[4]Co-first author

The authors declare no competing financial interests.

Introduction

Errors during movement have been studied empirically for the past two centuries (Meyer et al., 1988; Schmidt et al., 1979; Shadmehr et al., 2010; Woodworth, 1899), and it is evident from this literature that minimizing error depends on feedback loops that rely upon both external and internal feedback (Desmurget and Grafton, 2000; Miall, 1996). In the human motor system, a key source of external feedback is visual information, and studies have consistently shown that amplifying the gain of visual feedback improves motor performance by reducing errors during tasks such as drawing, force control, and arm pointing (Contreras-Vidal et al., 2002; Newell and Chew, 1975; Seidler et al., 2001; Sosnoff and Newell, 2005). Despite clear evidence that enhancing visual information about desired task-goals leads to improved motor performance, it is less clear what role cortical dynamics and connectivity observed within the cortex plays in this process.

There is ample evidence across numerous research modalities that the motor and parietal cortex are intricately and cooperatively involved in visually guided motor control (Caminiti et al., 1996; Clower et al., 1996; Dipietro et al., 2014; Jeannerod et al., 1995). Classic work showed that neurons in area 7 of the monkey respond during reaching movements to visual stimuli (Mountcastle et al., 1975). In humans, transcranial magnetic stimulation of the posterior parietal cortex has been used to disrupt visually guided reaching movements (Della-Maggiore et al., 2004; Desmurget et al., 1999). Neuroimaging in humans confirmed the role of both the motor cortex and parietal cortex in visually-guided motor control (Ellermann et al., 1998; Hamzei et al., 2002; Vaillancourt et al., 2003), and event-related potentials from the frontoparietal network measured using electroencephalography have been shown to correspond with sub-movements during visually-guided upper limb movements (Dipietro et al., 2014).

With regard to oscillatory activity in the motor cortex and parietal cortex, prior studies have examined oscillations at specific electrodes and reported event-related changes in spectral power in the beta-band that are specific to the stage of movement (Allen and MacKinnon, 2010; Kilavik et al., 2013; Pfurtscheller et al., 1994). Movement-related beta-band oscillations over the bilateral motor cortex exhibit a sharp decrease in spectral power at the beginning of a movement (Cruikshank et al., 2012; Gwin and Ferris, 2012; Kilavik et al., 2013; Pastötter et al., 2012) and beta-band activity increases near the end of the movement and was related to overall movement time (Ofori et al., 2015). In addition, Tan and colleagues (2014) have shown increased beta-band activity (post-movement event-related synchronization) following movements with small errors and decreased beta-band activity following movements with large errors.

Beta-band activity has also been shown to play a role in attentional processes (Sauseng and Klimesch, 2008; Wróbel et al., 2007). For instance, in the context of online motor control, attending to visual information about a task may also rely on beta-band causal influences from parietal areas. Recent studies have shown that increased sensory processing during behavioral tasks is dependent on the strength of parietal connections with frontal and sensorimotor areas (Akam and Kullmann, 2014; Hillebrand et al., 2012). However, it is difficult to distinguish attention-related processes from sensorimotor control (Engel and

Fries, 2010). Recent work suggests that beta-band activity functions to enhance gain of feedback loops at subsequent stages of visual information processing (Gola et al., 2013). Here we test the hypothesis that high visual feedback gain will reduce movement errors, enhance movement related beta-band desynchronization in the motor cortex, and alter directionally-specific connectivity between the parietal cortex and motor cortex.

Materials and Methods

Subjects

Sixteen participants (mean age: 29.4±3.8 yrs.; 6 females) were recruited for this study. All participants were young healthy right-handed individuals with normal or corrected vision. Participants were asked to refrain from consuming caffeine and using any hair products on the day of testing. Prior to experimental testing, participants provided informed consent. This experimental study was approved by the local Institutional Review Board.

Experimental Design and Task

The experimental setup for the movement task was similar to prior work (Ofori et al., 2015). Participants sat upright in a chair with their right arm supported against a cantilever beam attached to a custom-made manipulandum. Figure 1A depicts the general experimental procedures for the task sessions. Participants were instructed to perform rapid and accurate arm movements by flexing the elbow to 3 target angles (12°, 36°, and 72°) under two feedback conditions (low and high visual gain) while the experimenters monitored physiological and kinematic data (Figure 1A). Visual feedback about the participants' angular position was provided to the participant through a 30″ computer monitor (Dell UltraSharp U3011, Dell Co, Round Rock, TX).

As Figure 1 illustrates, the target location is depicted with a solid green H character, the start position is depicted with a solid gray H character, and a yellow X cursor depicts the current participant position. Visual gain was manipulated by changing the distance between the start and target position on the computer monitor. The high visual gain condition (17 cm / 6°) resulted in the distance between the start and target positions on the monitor to appear 25 times farther than the distance in the low visual gain condition (0.68 cm / 6°).

The time allotted for each trial was 12 sec. For the first 3 sec of a trial, the participants' right arm was at the start position. Then for the next 4 sec, the participants were asked to use their elbow flexors to move the manipulandum to the required distance as fast and accurately as possible after the participants heard the first 400 Hz auditory cue, and to keep the cursor in the middle of the target before the second auditory cue. Next, the participants heard a second auditory tone that cued them to return to the start position, and this period lasted 5 seconds. Only the first 7 sec of the 12 sec interval was analyzed. The experimental design resulted in 6 distinct conditions which include: 1) high visual gain feedback in short distance (12° target), 2) low visual gain feedback in short distance (12° target), 3) high visual gain feedback in medium distance (36° target), 4) low visual gain feedback in medium distance (36° target), 5) high visual gain in long distance (72° target), and 6) low visual gain feedback

in long distance (72° target). All participants performed 50 trials for each unique condition in a blocked design for a total of 300 trials. Block order was randomized across participants.

Data Acquisition

The MotionMonitor (Innovative Sports Training, Inc., Chicago, IL) system was configured to synchronize data in real time from electromyography (EMG), electroencephalography (EEG), and kinematic systems using an analogue sync pulse. The sync pulse was an analogue signal delivered to each data collection device, and all collected through the MotionMonitor software that was subsequently time-synced using the common analogue signal.

Kinematic data acquisition—The kinematic data were collected with an angular displacement transducer. The transducer was mounted at the axis of rotation of the manipulandum. An excitation voltage of 16 V from a Leader LPS-152 DC Tracking Power Supply (Advanced Test Equipment Rentals, San Diego, CA) that was used to power the angular displacement transducer. The displacement data were transmitted via a 16-bit A/D converter and digitized at 1000Hz using a USB-1616HS-BNC A/D board (Measurement Computing, Norton, MA).

EMG data acquisition—EMG data were collected with the Delsys Trigno Wireless System (Delsys Inc., Boston, MA). Participants were prepped by rubbing the desired locations on the right arm with alcohol. Four channels were used to measure electrophysiological activity from the muscle. The wireless EMG electrodes were placed at four locations on the participant's right arm. The four locations were the biceps brachii, brachioradialis, triceps lateral head and triceps long head. The EMG data were sampled at 1000 Hz.

EEG data acquisition—EEG data were collected with the ActiveTwo system that was comprised of 128 Ag-AgCl Active Two electrodes. The active electrodes were connected to a cap that was in a preconfigured montage covering the entire scalp. The signals were amplified through the electrodes at the source and had an output impedance of <1 ohm.

EEG signals were digitally amplified at DC and sampled at 2,048 Hz. Electrical potentials were recorded between each electrode and Common Mode Sense (CMS) active electrode and Driven Right Leg (DRL) passive electrode located at the center of the scalp in relation to all to other electrodes. The CMS and DRL electrodes were used to drive the average potential of the subject as close as possible to the AD-box reference potential electrode. The electrode offsets, a running average of the voltage measured between the CMS and each active electrode, were evaluated before the start of each condition and during data collection to be within the acceptable range of 40 μV. The electrode offset served as an indirect measure of impedance tolerance. To ensure that a stable and high quality signal was recorded from each active electrode throughout the recording session, the electrode offset was monitored.

Data Processing and Analysis

All behavioral and electrophysiological data were imported into MATLAB 2014 (The Mathworks, Natick, MA). Angular position data were lowpass filtered at 30 Hz (Butterworth 4th order dual pass). Velocity and acceleration were obtained based on the differential of the angular position signal.

Two movement phases were identified: movement onset phase and post ballistic movement (PBM) phase. The movement onset was determined from the acceleration data. This was accomplished by searching backwards from peak acceleration until the acceleration data were 5% of the peak acceleration. The start of post ballistic movement (PBM) phase was defined as the first zero velocity after peak velocity. The PBM phase duration was defined as 2 seconds from the start of PBM phase.

Kinematic analysis—Kinematic data were comprised of peak displacement, peak velocity, peak acceleration, time to peak velocity time, time to peak acceleration, and time to peak deceleration during the movement onset phase. Task performance data was assessed with Root Mean Square Error (RMSE), standard deviation of angular displacement (SD), number of zero-crossings of acceleration data, zero-crossing start time, and average acceleration during the PBM phase over a 2 s period. RMSE of angular displacement during the PBM phase was computed similar to a measure of SD but the target was used as the reference instead of the mean. SD was defined as the standard deviation of angular displacement during the PBM phase. The number of zero-crossings was quantified by the number of changes in the direction of acceleration during the PBM phase. Zero-crossing start time was computed as the first zero velocity after peak velocity (i.e., beginning of the PBM phase). The average acceleration was computed as the average of the absolute value of acceleration.

EMG analysis—EMG data were highpass filtered at 2 Hz (Butterworth 4th order dual pass) to remove the DC offset, rectified, and then lowpass filtered at 50 Hz (Butterworth 2th order dual pass). Mean EMG for each muscle group (i.e., biceps, brachioradialis, triceps lateral head and triceps long head) was computed during the PBM phase (Figure 1B).

EEG preprocessing—EEG data were processed using custom routines based on EEGLAB used in previous work (Ofori et al., 2015). First, EEG data were bandpass filtered between 1 and 70 Hz. EEG data underwent a channel interpolation procedure for EEG channels with large fluctuations (> 4 SD). On an average, two channels per trial per subject were interpolated. The EEG signals were then re-referenced to the global average of all EEG channels. EEG data epochs were extracted from 1 s before movement onset to 3 seconds after movement onset for all trials. EEG data was prepared for further analysis by concatenating all epochs within each condition within each participant. The concatenated data were decomposed using independent component analysis (ICA).

EEG source localization—Infomax ICA using EEGLAB routines decomposed the data into independent components for each individual. DIPFIT functions within EEGLAB were used to compute an equivalent current dipole model that best explained the scalp topography

of each independent component. Each dipole was identified through a finite element spherical head model from Brain Electrical Source Analysis [BESA (BESA GmbH, Grafelfing, GE)]. We localized the electrodes using a preconfigured montage from the subjects published in previous work (Poon et al., 2012). In the previous work, we used a digitization apparatus to identify Cartesian and polar coordinates of the subjects for the 128 electrode montage. The digitization apparatus for 3D digitization used in previous work was the Polhemus Patriot (Polhemus, Colchester, Vermont). The digitized electrode locations were aligned with the head and then these coordinates were converted to normalized Montreal Neurological Institute (MNI) space. Independent components were excluded if the projection of the equivalent current dipole to the scalp accounted for more than 10% of the residual variance, was outside of the brain, or if the time-course, spectra, and topography of ICs were reflective of eye movement or electromyography artifact (Ofori et al., 2015).

EEG Measure Projection Analysis—Measure projection analysis (MPA) is a statistical method for characterizing the localization and consistency of EEG measures across sessions of EEG recordings (Bigdely-Shamlo et al., 2013). It allows the use of EEG as a 3D cortical imaging modality with near-cm scale spatial resolution. MPA identifies domains and defines anatomical regions of interest (ROIs) and finds ratios of domain masses for cortical structures which incorporates the probabilistic atlas of human cortical structures provided by the Laboratory of NeuroImaging (LONI) project (Shattuck et al., 2008). This procedure clusters domains based on measure specific data from all individual subject IC locations. These domains are identified in a data-driven manner with unique EEG measure (e.g., ERSP) time-frequency features in 3D space. To create the domains, a cubic space grid with 8-mm spacing was situated in the brain volume in MNI space which served as the MPA brain model. Voxels outside the brain model were excluded. Local convergence values were calculated based on the algorithm explained in detail by Bigdely and colleagues (2013). Local convergence helps deal with the multiple comparisons problem by finding measure similarity of dipoles and comparing them with randomized dipoles. A pair wise IC similarity matrix was constructed by estimating the signed mutual information between independent component-pair event-related power spectral perturbation (ERSP) measure vectors using a Gaussian distribution assumption. Signed mutual information was estimated to improve the spatial smoothness of obtained MPA significance values (Bigdely-Shamlo et al., 2013). A significance threshold for convergence at each brain location was obtained by bootstrap statistics. The raw voxel significance threshold was set to $p<0.001$, which is based on prior studies in the literature (Bigdely-Shamlo et al., 2013; Misra et al., 2016).

Within each domain, ERSPs were computed for each condition to identify region-specific and frequency-specific oscillatory activity during the movement. Theta (4–8 Hz), alpha (8–12 Hz), beta (13–30 Hz), and gamma (31–50 Hz) bands were examined. For each identified domain, significant differences in the power at each frequency band (between high and low visual gain conditions and at each of the three distances) were computed by first projecting the ERSP associated with each condition to each voxel in a domain. This produced a projected measure. Next, a weighted-mean measure across all domain voxels was weighted by the dipole density of an individual voxel per participant. The measure was then normalized by the total domain voxel density. Analysis of projected source measures were

separated into distinct spatial domains by threshold-based Affinity Propagation clustering based on a similarity matrix of pair-wise correlations between ERSP measure values for each position. For the current study, the maximal exemplar-pair similarity, a parameter that ranges from 0 – 1.0 was set to a value of 0.8 based on prior work (Bigdely-Shamlo et al., 2013; Ofori et al., 2015).

EEG Connectivity Analysis—ICs used for connectivity analysis were selected from domains revealed by MPA analysis. Routines from the SIFT toolbox were used to model the multivariate causal interactions between epoched IC time-series (Delorme et al., 2011; Iversen et al., 2014). Specifically, for each subject and condition, ICs were pre-processed with a piecewise detrending method with a segment length of 400 ms and a stepsize of 100 ms to remove drift, followed by a temporal and ensemble normalization. Subject-specific linear vector autoregressive (VAR) models (orders ranging from 20 to 30) were then fit to the multi-trial ensemble, in a 400 ms sliding window with a step size of 50 ms, using the Vieira-Morf lattice algorithm. Subsequently, model validation tests (i.e., autocorrelation and Portmanteau) were conducted to check the residuals of the model for serial and cross-correlation, and the stability of the model of VAR coefficients. The direct directed transfer function with full causal normalization (dDTF) was estimated from the VAR coefficients. The dDTF captures frequency-domain conditional connectivity and reflects only direct causal flows between two signals. The dDTF is a product of partial directed coherence and the full-frequency directed transfer function and denoted by the following equation:

$$\delta_{\mathrm{ij}}^2(f)=\frac{|H_{\mathrm{ij}}(f)|^2}{\sum_f\sum_{k=1}^{M}|H_{\mathrm{ik}}(f)|^2}P_{\mathrm{ij}}^2(f)$$

where *H(f)* is the MVAR transfer matrix and *P(f)* is the partial coherence at a given frequency. dDTF is similar to conditional spectral Granger causality as it quantifies directionally specific information transfer between source processes at each frequency (Delorme et al., 2011). Bootstrap resampling was performed to approximate the distribution of the connectivity estimator (i.e., dDTF). Each unique condition for each subject was resampled 200 times. Each unique IC couple representing the domain to domain connectivity for each subject was averaged within subject to generate a unique 1 to 1 time by frequency connectivity matrix to reduce varying dipole dimensionality across subjects. Each individual subject bootstrap estimated dDTF matrix for the parietal to motor areas and motor to parietal areas underwent non-parametric statistical analysis to determine differences across gain.

Statistical analysis

A repeated measures ANOVA was used for the kinematics and EMG variables. If the distribution departed from normality, log transformation was used. We then FDR corrected the p-values at $p < 0.05$, to control for multiple comparisons (Benjamini and Hochberg, 1995). For EEG ERSP measures, a non-parametric boostrapped t-test was performed at each distance comparing high gain to low gain. For EEG connectivity measures, a non-parametric boostrapped t-test was performed at each distance comparing high gain to low gain. For both

ERSP and connectivity measures, p-values were then FDR corrected to $p < 0.05$, controlling for multiple comparisons across the whole time-frequency matrix.

Correlation analysis

A Spearman Rho correlation matrix was computed between all subjects and all conditions (16 subjects x 6 conditions = 96 per time-frequency cell) in the ERSP versus connectivity at each time-frequency cell. The p-values were FDR corrected $p < 0.05$. A goal also was to determine if there was an association between movement error during the PBM phase and beta-band activity in the two domains. Beta-band ERSP values were extracted in the 13–30 Hz range for 0.5s after the beginning of the PBM phase. The average beta-band ERSP values were computed across trials, and then the data points for all subjects and conditions ($16 \times 6 = 96$) were compared with RMSE. We conducted a Spearman Rho correlation between RMSE and across trials mean beta-band ERSP for each domain.

Results

Kinematic data

As expected, significant distance-effects were found on the following variables during the movement onset phase: peak displacement, peak velocity, peak acceleration, peak velocity time, peak acceleration time, and peak deceleration time. The pattern of results across the aforementioned dependent variables mainly indicated that the long distance resulted in faster and longer duration movements (Table 1). Only peak displacement during the movement onset phase was influenced by visual gain, such that high gain led to shorter movements by approximately 1 degree at each distance. Since velocity and acceleration during the movement onset phase were not affected by visual gain, these potential mediating factors were minimized in the experiment.

Statistical analysis revealed significant distance-effects on the following variables during the PBM phase (Table 1): average acceleration, SD of angular position, number of zero-crossings of acceleration, and zero-crossing start time. The pattern of results showed that the long distance was associated of a delayed onset of the PBM phase, increased average acceleration of movement and SD of movement position, and reduced number of zero-crossings (Table 1).

Statistical analysis revealed significant gain-effects on the following variables during the PBM phase (Table 1): average acceleration, RMSE of angular position, number of zero-crossings of acceleration, SD of angular position, and zero-crossing start time (Figure 2). The results mainly revealed increased movement corrections (i.e., number of zero-crossings and average acceleration) and reduced movement error (i.e., RMSE) and variability (i.e., SD) in the high gain condition compared with the low gain condition.

All distance by gain interaction effects were not significant, with the exception of the SD during the PBM phase. Post hoc paired t-tests at each distance revealed that SD for low visual gain conditions was lower than high visual gain at the short distance ($p= 0.003$) and medium distance ($p= 0.015$), but not the long distance ($p= 0.227$).

EMG data

Statistical analysis revealed significant distance-effects were found on the following variables during the PBM phase: biceps and brachioradialis mean EMG. The pattern of results mainly indicated that the longer distance resulted in higher mean EMG during the PBM phase. (Table 1).

Statistical analysis revealed significantly increased EMG activity in high visual gain compared with low visual gain during the PBM phase for the biceps, brachioradialis, and triceps lateral head. There were no significant visual gain × distance interactions in the mean EMG (Table 1).

EEG data

Figure 3A shows the ERSP time-frequency plot from a dipole located in the sensorimotor area for one subject. This subject specific data is unique to the sensorimotor area, and clustering with MPA analysis (see Figure 3B) can help reduce the dimensionality that occurs with source localization from subjects with varying dipole location distributions. Figure 3B shows the sensorimotor domain and ERSP time-frequency plots for high and low visual gain conditions across subjects. The locations and nomenclature of domains are based on the Laboratory of NeuroImaging (LONI) project probabilistic atlas (Shattuck et al., 2008). Figure 4 contains the time-frequency contrasts for visual gain at each distance for the identified common source domains revealed by MPA and the corresponding Brodmann areas are shown in Figure 4A and 4B.

Figure 4A shows a left sensorimotor area domain that is consistent with primary and - somatosensory cortex (BA 2 and 3), primary motor cortex (BA 4) and spatial, and sematic processing cortex (BA 40). Also shown is the statistically thresholded differences between time frequency plots for the visual gains (high vs. low), at each of the three distances (short, medium, and long): high visual gain vs. low visual gain at the short distance, high visual gain vs. low visual gain at the medium distance, and high visual gain vs. low visual gain at the long distance. Statistical analysis revealed that high visual gain had decreased spectral power (i.e. greater desynchronization) in the alpha- and beta-band compared to low visual gain during the PBM phase across all distance conditions [t(15)'s, FDR p's ≤ 0.05]. Common time-frequency statistical results are displayed in the Overlap ERSP contrast plot for Figure 4A. The common overlap results show spectral changes occurring in theta- and beta-band approximately 500 ms after the onset of the PBM phase, and changes in alpha and beta 1000 ms after the onset of the PBM phase.

Figure 4B shows a parietal area domain that is consistent with BA 31, BA 23, and BA 7 and shows the statistical comparison of time-frequency plots for the visual gains (high vs. low) compared at the three distances (short, medium, and long): high visual gain vs. low visual gain at the short distance, high visual gain vs. low visual gain at the medium distance, and high visual gain vs. low visual gain at long distance. Statistical analysis revealed that high visual gain had decreased spectral power across multiple frequencies compared to low visual gain during the PBM phase across all distance conditions [t(15)'s, FDR p's ≤ 0.05]. Common time-frequency statistical results are displayed in the Overlap ERSP contrast plot

for Figure 4B. The results show common decreases in spectral power across distances occurring in alpha-band at the start of the PBM phase, common decreases in spectral power in alpha- and beta-bands occurring 500 ms after the onset of the PBM phase, and theta, alpha, and beta spectral power decreases occurring 1000 ms after the onset of the PBM phase.

Figure 5 shows the group statistical comparison of connectivity as measured by dDTF from IC located in the medial parietal cortex to the motor cortex for the different visual gains compared across the short, medium, and long distance conditions. Increased connectivity in the high gain versus low gain condition is indicated by red color whereas decreased connectivity is illustrated with blue color [t(15)'s, FDR p's < 0.05]. Statistical analyses revealed increased connectivity in the high gain condition compared with the low gain condition for the short distance in theta-band at movement onset, at the beginning of the PBM phase, and later in the PBM phase. We also observe increased connectivity in high gain versus low gain in the beta-band during the PMB phase for the short, medium, and long distances. When examining connectivity from the left sensorimotor area to the parietal area, there were no statistical differences across gain at all three distances [t(15)'s, FDR p's > 0.05]. This suggests a directionally-specific effect of gain on connectivity from the parietal cortex to the sensorimotor cortex.

Correlation analysis

There were no significant correlations between ERSP and connectivity from parietal cortex to sensorimotor cortex (FDR p's > 0.05). The correlation between RMSE and beta-band of ERSP during the PBM phase at each domain resulted in a significant association. There was a significant positive, and low-moderate correlation between beta-band of ERSP and RMSE during the PBM phase at each domain (Domain 1 Rho = 0.425; $p < 0.001$; Domain 2 Rho = 0.441; $p < 0.001$).

Discussion

We investigated how manipulating visual feedback and movement distance relates to cortical dynamics and neuromuscular activity during ballistic movements of the upper limb. We present three novel observations. First, high visual gain resulted in decreased motor error and was associated with increased beta-band desynchronization within parietal cortex and contralateral sensorimotor cortex during the PBM phase when compared to low visual gain. This observation was found across all distances. Second, high visual gain also resulted in increased theta-band and alpha-band desynchronization within parietal and contralateral sensorimotor cortex during the PBM phase. Third, we observed increased beta-band connectivity from the parietal cortex to the sensorimotor cortex during high gain compared with low gain conditions at all distances. These observations were not found from sensorimotor cortex to parietal cortex, suggesting a directionally-specific nature to the changes in connectivity. These new findings provide support for the interpretation that broad-band oscillations across sensorimotor and parietal cortex coordinate to facilitate accurate upper limb movement.

Beta-band activity and task-related motor performance

Desynchronization represents a decrease in the power of oscillatory EEG activity, and reflects a state of active cortical processing during movement execution and imagery of movements (Gerloff et al., 1998; Leocani et al., 2001, 2000; Ofori et al., 2015; Pfurtscheller and Lopes da Silva, 1999; Szurhaj et al., 2003). Pfurtscheller and Lopes da Silva (1999) noted that event-related desynchronization or synchronization represents alterations in the activity of local populations of neurons and interneurons in neural networks. Desynchronization has been associated with more efficient task performance, and more cell assembly involvement in information processing (Pfurtscheller and Lopes da Silva, 1999).

Cortical beta amplitude has been studied as a crucial factor that regulates motor performance within and between trials (Boonstra et al., 2007; Gilbertson et al., 2005; Meyniel and Pessiglione, 2014; Serrien and Brown, 2003; Tan et al., 2014). For instance, Lin and colleagues (2012) compared haptic feedback to non-haptic feedback in a visuomotor tracking task and found haptic feedback results in less tracking error with desynchronization in beta-band of the right occipital cortex. Tan and colleagues (2014) have recently shown with a hand-controlled joystick task that increased beta-band activity may reflect neural processes that evaluate the actual movement performed with the intended movement outcome. The authors indicate that increases in beta-band activity occur in trials with small errors, whereas trials with larger errors had decreases in beta-band activity. The findings from the current study extend the results from Tan and colleagues (2014) in two novel ways. First, we examined an upper limb movement task, and the changes in error that we induced were due to changes in the gain of visual feedback. Second, we found that increased visual feedback led to increased beta-band desynchronization in the motor cortex and parietal cortex mainly during the PBM phase, which allowed for better motor performance (i.e., to reduce angular error). Visually-guided upper limb movements seem to be performed with the least error when beta-band activity remains decreased during the post-ballistic movement (PBM) phase.

Clinically, increases and decreases in beta-band activity have been studied in people with Parkinson’s disease (Hammond et al., 2007; Kühn et al., 2004). Bradykinesia in patients with Parkinson’s disease is correlated with increases in beta-band activity (Hammond et al., 2007; Kühn et al., 2008). In studies of high-frequency deep brain stimulation of the subthalamic nucleus, Kühn and colleagues (2008) suggested that deep brain stimulation leads to a reduction of synchronization in the beta-band of motor cortex and better task performance. It is theorized that beta-band activity functions to promote the status quo (Engel and Fries, 2010), or in the current context motor cortex integrates beta-band cortical activity from parietal area for accurate motor performance.

Beta-band activity and attentional processing

The posterior parietal cortex, dorsal premotor cortex, and motor cortex play a key role during online motor corrections (Archambault et al., 2015; Battaglia-Mayer et al., 2014). Our study found a directionally-specific increase in beta-band connectivity from parietal cortex to motor cortex during high visual gain conditions. Dipietro and colleagues (2014) have shown that the timing of event related potential (ERP) in the frontoparietal network

relate to submovements during visually-guided movement. The analysis of the time lag of activity between motor cortex and parietal cortex in primates has revealed that the motor cortex is activated earlier than the parietal cortex during control of hand movement (Archambault et al., 2011). We extended these studies to consider the result of connectivity between the two cortical domains. In this study, we used the direct directed transfer function with full causal normalization (dDTF) for computing connectivity between motor cortex and parietal cortex, and found that gain affects connectivity only in the direction of parietal cortex to motor cortex. The effect of gain on dDTF was not significant when examining motor cortex to parietal connectivity across all frequencies, suggesting specificity in the direction of connectivity for the influence of visual gain.

It is proposed that beta-band activity increases the sensitivity for visual input during high attentional demanding tasks (Gola et al., 2013). It has been previously shown that attending to visual information increases local field potentials in primary and medial visual centers in cats (Wróbel et al., 2007). In addition, work in macaques has shown increased beta-band parietal casual influence to the sensorimotor cortex during a GO/NO-GO visual pattern discrimination task (Brovelli et al., 2004). In line with previous studies, the current study reports increased beta-band connectivity from parietal to motor cortical areas during the correction phase of the movement for high visual gain conditions. This suggests that during local sustained beta-band desynchronization, the motor cortex may be receiving input in the beta-band from the medial parietal cortex. Beta-band in the sensorimotor system may serve as a binding mechanism to achieve the status quo or to enhance motor performance (Engel and Fries, 2010). Our findings suggest that electrophysiological activity during the task is more than likely functional and the error monitoring system an individual employs must engage distinct cortical areas in order to achieve task goals. We provide new evidence that errors are not a result of momentary fluctuations in brain activity, but rather suggest that errors that manifest in the execution of the descending commands are a result of a mechanism that coordinates domain-specific beta-band activity for tasks that may require additional attentional resources.

Findings from the current study are similar to studies that suggest beta-band oscillations play an active role in the motor cortex (Brinkman et al., 2014; Ofori et al., 2015; Pfurtscheller et al., 1994) and reinforce that parietal to motor cortex connectivity is important for sensorimotor integration in contexts with high visual information (Vukelić et al., 2014). Our findings extend the hypothesis that cortical oscillations in the beta-band are selectively related to attention and beta-band activity and connectivity may serve to select relevant task information. The findings suggest that visual gain affects connectivity from the medial parietal cortex to sensorimotor cortex, and not from sensorimotor cortex to parietal cortex, and thus may reflect a cortical mechanism that is crucial to sensorimotor integration and modulating neuromuscular activity.

Theta-band and alpha-band activity

In addition to observations in the beta-band, we found evidence that high gain led to increased desynchronization in the theta-band and alpha-band ERSP activity at each movement distance (Figure 4). The differences in the alpha-band across gain were observed

earlier in the overlap analysis in the parietal domain than in the sensorimotor domain. Recent theoretical models for alpha oscillations suggest that alpha event-related synchronization reflects inhibition, and a decrease in the amplitude of alpha-band activity reflects a release from inhibition (Klimesch, 2012). Ofori and colleagues (2015) supported this during an upper limb movement task as the authors found alpha-band power decreased during the movement, and the current paper found a similar observation (Figure 3). The novel finding here is that visual gain modulated the level of desynchronization, mainly after the ballistic phase of the movement had ended. In the theta-band, Ofori and colleagues (2015) found that movement acceleration related to theta-band activity in the contralateral sensorimotor domain. The current paper observed the same theta-band synchronization at the beginning of movement (Figure 3), but visual gain did not alter the level of theta-band activity at movement onset. It was not until during the PBM phase did we observe that theta-band activity was affected by visual gain. Thus, the current findings suggest a broad-band desynchronization during the PBM phase across theta-, alpha-, and beta-band in the sensorimotor and parietal domains.

Effects of visual gain on neuromuscular activity

The hypothesis that beta-band desynchronization is a mechanism of the motor cortex to mediate neuromuscular activity of the agonist and antagonist muscles can be gleaned from literature on PD and stroke (Bagce et al., 2012; Baroni et al., 1984). Baroni and colleagues (1984) have shown that L-dopa treatment increased EMG activity and reduced errors in a ballistic arm movement task. Increased muscle activity during flexion of the index finger to a target was found in stroke survivors in conditions with increased visual gain and low error (Bagce et al., 2012). The authors also found increased M1 excitability with increased visual feedback. Increased visual feedback typically leads to reduced performance error. Our results suggest that M1 excitability involves not only regional changes in beta-band desynchronization but also changes in connectivity from the parietal cortex. Thus, neurological diseases that exhibit increased movement error may be due to a sensorimotor integration problem that may be a result of altered desynchronization or cortico-cortico connectivity. This selective role of beta-band desynchronization and connectivity of the motor cortex and sensory information highlights its importance in mediating performance error.

In the current study, visual information was used to alter movement error and it was found that movement errors were reduced and the number of zero-crossings increased with enhanced visual information. It is well established that the agonist and antagonist muscle have a burst of activity as the limb approaches the target and complete the 2nd and 3rd phase of the triphasic-EMG pattern (Gottlieb et al., 1996). The triphasic pattern was evidenced in the current study (Figure 1), and the new finding was that the agonist and antagonist muscles displayed increased activity during the PBM phase with enhanced visual gain.

We conclude that the regulation of regional beta-band activity and beta-band connectivity between parietal and motor cortex are critical for individuals to perform well in environments with various scales of visual information. We observed changes in desynchronization in beta-band in the left sensorimotor cortex and the parietal cortex.

Further, we found that theta-band and alpha-band oscillations had increased desynchronization at high visual gain, suggesting that a broad-band suppression of the oscillations with high gain. This desynchronization occurred after the ballistic movement, and only during the PBM phase. Finally, parietal to sensorimotor cortex connectivity was influenced by visual gain, with high gain resulting in increased connectivity in the beta-band at all distances. Our findings suggest that the motor cortex uses distinct oscillatory, broad-band activity regionally and between relevant cortical networks to optimize motor performance when humans are making corrections. Our findings also highlight the importance of the state of the motor cortex and propose that theta-, alpha-, and beta-band may serve as a binding mechanism for visual information during motor corrections.

Acknowledgments

This work was supported by NINDS R01 NS058487, R01 NS052318, and T32 NS082169.

References

Akam T, Kullmann DM. Oscillatory multiplexing of population codes for selective communication in the mammalian brain. Nat. Rev. Neurosci. 2014; 15:111–122. [PubMed: 24434912]

Allen DP, MacKinnon CD. Time-frequency analysis of movement-related spectral power in EEG during repetitive movements: a comparison of methods. J. Neurosci. Methods. 2010; 186:107–115. [PubMed: 19909774]

Archambault PS, Ferrari-Toniolo S, Battaglia-Mayer A. Online Control of Hand Trajectory and Evolution of Motor Intention in the Parietofrontal System. J. Neurosci. 2011; 31:742–752. [PubMed: 21228183]

Archambault PS, Ferrari-Toniolo S, Caminiti R, Battaglia-Mayer A. Visually-guided correction of hand reaching movements: The neurophysiological bases in the cerebral cortex. Vision Res., Online Visual Control of Action. 2015; 110(Part B):244–256.

Bagce HF, Saleh S, Adamovich SV, Tunik E. Visuomotor Gain Distortion Alters Online Motor Performance and Enhances Primary Motor Cortex Excitability in Patients with Stroke. Neuromodulation J. Int. Neuromodulation Soc. 2012; 15:361–366.

Baroni A, Benvenuti F, Fantini L, Pantaleo T, Urbani F. Human ballistic arm abduction movements Effects of L-dopa treatment in Parkinson's disease. Neurology. 1984; 34:868–868. [PubMed: 6539863]

Battaglia-Mayer A, Buiatti T, Caminiti R, Ferraina S, Lacquaniti F, Shallice T. Correction and suppression of reaching movements in the cerebral cortex: Physiological and neuropsychological aspects. Neurosci. Biobehav. Rev. 2014; 42:232–251. [PubMed: 24631852]

Benjamini Y, Hochberg Y. Controlling the False Discovery Rate: A Practical and Powerful Approach to Multiple Testing. J. R. Stat. Soc. Ser. B Methodol. 1995; 57:289–300.

Bigdely-Shamlo N, Mullen T, Kreutz-Delgado K, Makeig S. Measure projection analysis: a probabilistic approach to EEG source comparison and multi-subject inference. NeuroImage. 2013; 72:287–303. [PubMed: 23370059]

Boonstra TW, Daffertshofer A, Breakspear M, Beek PJ. Multivariate time-frequency analysis of electromagnetic brain activity during bimanual motor learning. NeuroImage. 2007; 36:370–377. [PubMed: 17462913]

Brinkman L, Stolk A, Dijkerman HC, de Lange FP, Toni I. Distinct Roles for Alpha- and Beta-Band Oscillations during Mental Simulation of Goal-Directed Actions. J. Neurosci. 2014; 34:14783–14792. [PubMed: 25355230]

Brovelli A, Ding M, Ledberg A, Chen Y, Nakamura R, Bressler SL. Beta oscillations in a large-scale sensorimotor cortical network: Directional influences revealed by Granger causality. Proc. Natl. Acad. Sci. U. S. A. 2004; 101:9849–9854. [PubMed: 15210971]

Caminiti R, Ferraina S, Johnson PB. The Sources of Visual Information to the Primate Frontal Lobe: A Novel Role for the Superior Parietal Lobule. Cereb. Cortex. 1996; 6:319–328. [PubMed: 8670660]

Clower DM, Hoffman JM, Votaw JR, Faber TL, Woods RP, Alexander GE. Role of posterior parietal cortex in the recalibration of visually guided reaching. Nature. 1996; 383:618–621. [PubMed: 8857536]

Contreras-Vidal JL, Teulings H-L, Stelmach GE, Adler CH. Adaptation to changes in vertical display gain during handwriting in Parkinson's disease patients, elderly and young controls. Parkinsonism Relat. Disord. 2002; 9:77–84. [PubMed: 12473396]

Cruikshank LC, Singhal A, Hueppelsheuser M, Caplan JB. Theta oscillations reflect a putative neural mechanism for human sensorimotor integration. J. Neurophysiol. 2012; 107:65–77. [PubMed: 21975453]

Della-Maggiore V, Malfait N, Ostry DJ, Paus T. Stimulation of the Posterior Parietal Cortex Interferes with Arm Trajectory Adjustments during the Learning of New Dynamics. J. Neurosci. 2004; 24:9971–9976. [PubMed: 15525782]

Delorme A, Mullen T, Kothe C, Akalin Acar Z, Bigdely-Shamlo N, Vankov A, Makeig S. EEGLAB, SIFT, NFT, BCILAB, and ERICA: New Tools for Advanced EEG Processing. Comput. Intell. Neurosci. 2011; 2011

Desmurget M, Epstein CM, Turner RS, Prablanc C, Alexander GE, Grafton ST. Role of the posterior parietal cortex in updating reaching movements to a visual target. Nat. Neurosci. 1999; 2:563–567. [PubMed: 10448222]

Desmurget M, Grafton S. Forward modeling allows feedback control for fast reaching movements. Trends Cogn. Sci. 2000; 4:423–431. [PubMed: 11058820]

Dipietro L, Poizner H, Krebs HI. Spatiotemporal Dynamics of Online Motor Correction Processing Revealed by High-density Electroencephalography. J. Cogn. Neurosci. 2014; 26:1966–1980. [PubMed: 24564462]

Ellermann JM, Siegal JD, Strupp JP, Ebner TJ, Ugurbil K. Activation of Visuomotor Systems during Visually Guided Movements: A Functional MRI Study. J. Magn. Reson. 1998; 131:272–285. [PubMed: 9571103]

Engel AK, Fries P. Beta-band oscillations — signalling the status quo? Curr. Opin. Neurobiol., Cognitive neuroscience. 2010; 20:156–165.

Gerloff C, Richard J, Hadley J, Schulman AE, Honda M, Hallett M. Functional coupling and regional activation of human cortical motor areas during simple, internally paced and externally paced finger movements. Brain J. Neurol. 1998; 121:1513–1531.

Gilbertson T, Lalo E, Doyle L, Di Lazzaro V, Cioni B, Brown P. Existing motor state is favored at the expense of new movement during 13–35 Hz oscillatory synchrony in the human corticospinal system. J. Neurosci. Off. J. Soc. Neurosci. 2005; 25:7771–7779.

Gola M, Magnuski M, Szumska I, Wróbel A. EEG beta band activity is related to attention and attentional deficits in the visual performance of elderly subjects. Int. J. Psychophysiol., Psychophysiology in Australasia - ASP conference - November 28–30 2012. 2013; 89:334–341.

Gottlieb GL, Song Q, Hong DA, Corcos DM. Coordinating two degrees of freedom during human arm movement: load and speed invariance of relative joint torques. J. Neurophysiol. 1996; 76:3196–3206. [PubMed: 8930266]

Gwin JT, Ferris DP. An EEG-based study of discrete isometric and isotonic human lower limb muscle contractions. J. NeuroEngineering Rehabil. 2012; 9:35.

Hammond C, Bergman H, Brown P. Pathological synchronization in Parkinson's disease: networks, models and treatments. Trends Neurosci., July INMED/TINS special issue— Physiogenic and pathogenic oscillations: the beauty and the beast. 2007; 30:357–364.

Hamzei F, Dettmers C, Rzanny R, Liepert J, Büchel C, Weiller C. Reduction of Excitability ("Inhibition") in the Ipsilateral Primary Motor Cortex Is Mirrored by fMRI Signal Decreases. NeuroImage. 2002; 17:490–496. [PubMed: 12482101]

Hillebrand A, Barnes GR, Bosboom JL, Berendse HW, Stam CJ. Frequency-dependent functional connectivity within resting-state networks: An atlas-based MEG beamformer solution. Neuroimage. 2012; 59:3909–3921. [PubMed: 22122866]

Iversen, JR.; Ojeda, A.; Mullen, T.; Plank, M.; Snider, J.; Cauwenberghs, G.; Poizner, H. Causal analysis of cortical networks involved in reaching to spatial targets, in: 2014 36th Annual International Conference of the IEEE Engineering in Medicine and Biology Society (EMBC). Presented at the 2014 36th Annual International Conference of the IEEE Engineering in Medicine and Biology Society (EMBC; 2014. p. 4399-4402.

Jeannerod M, Arbib MA, Rizzolatti G, Sakata H. Grasping objects: the cortical mechanisms of visuomotor transformation. Trends Neurosci. 1995; 18:314–320. [PubMed: 7571012]

Kilavik BE, Zaepffel M, Brovelli A, MacKay WA, Riehle A. The ups and downs of beta oscillations in sensorimotor cortex. Exp. Neurol., Special Issue: Neuronal oscillations in movement disorders. 2013; 245:15–26.

Klimesch W. Alpha-band oscillations, attention, and controlled access to stored information. Trends Cogn. Sci. 2012; 16:606–617. [PubMed: 23141428]

Kühn AA, Kempf F, Brücke C, Doyle LG, Martinez-Torres I, Pogosyan A, Trottenberg T, Kupsch A, Schneider G-H, Hariz MI, Vandenberghe W, Nuttin B, Brown P. High-Frequency Stimulation of the Subthalamic Nucleus Suppresses Oscillatory β Activity in Patients with Parkinson's Disease in Parallel with Improvement in Motor Performance. J. Neurosci. 2008; 28:6165–6173. [PubMed: 18550758]

Kühn AA, Williams D, Kupsch A, Limousin P, Hariz M, Schneider G-H, Yarrow K, Brown P. Event-related beta desynchronization in human subthalamic nucleus correlates with motor performance. Brain. 2004; 127:735–746. [PubMed: 14960502]

Leocani L, Cohen LG, Wassermann EM, Ikoma K, Hallett M. Human corticospinal excitability evaluated with transcranial magnetic stimulation during different reaction time paradigms. Brain J. Neurol. 2000; 123:1161–1173.

Leocani L, Toro C, Zhuang P, Gerloff C, Hallett M. Event-related desynchronization in reaction time paradigms: a comparison with event-related potentials and corticospinal excitability. Clin. Neurophysiol. Off. J. Int. Fed. Clin. Neurophysiol. 2001; 112:923–930.

Lin C-L, Shaw F-Z, Young K-Y, Lin C-T, Jung T-P. EEG correlates of haptic feedback in a visuomotor tracking task. NeuroImage. 2012; 60:2258–2273. [PubMed: 22348883]

Meyer DE, Abrams RA, Kornblum S, Wright CE, Smith JE. Optimality in human motor performance: ideal control of rapid aimed movements. Psychol. Rev. 1988; 95:340–370. [PubMed: 3406245]

Meyniel F, Pessiglione M. Better Get Back to Work: A Role for Motor Beta Desynchronization in Incentive Motivation. J. Neurosci. 2014; 34:1–9. [PubMed: 24381263]

Miall RC. Task-dependent changes in visual feedback control: a frequency analysis of human manual tracking. J. Mot. Behav. 1996; 28:125–135. [PubMed: 12529214]

Misra G, Ofori E, Chung JW, Coombes SA. Pain-Related Suppression of Beta Oscillations Facilitates Voluntary Movement. Cereb. Cortex bhw061. 2016

Mountcastle VB, Lynch JC, Georgopoulos A, Sakata H, Acuna C. Posterior parietal association cortex of the monkey: command functions for operations within extrapersonal space. J. Neurophysiol. 1975; 38:871–908. [PubMed: 808592]

Newell KM, Chew RA. Visual Feedback and Positioning Movements. J. Mot. Behav. 1975; 7:153–158. [PubMed: 23947442]

Ofori E, Coombes SA, Vaillancourt DE. 3D Cortical electrophysiology of ballistic upper limb movement in humans. NeuroImage. 2015; 115:30–41. [PubMed: 25929620]

Pastötter B, Berchtold F, Bäuml K-HT. Oscillatory correlates of controlled speed-accuracy tradeoff in a response-conflict task. Hum. Brain Mapp. 2012; 33:1834–1849. [PubMed: 21618665]

Pfurtscheller G, Flotzinger D, Neuper C. Differentiation between finger, toe and tongue movement in man based on 40 Hz EEG. Electroencephalogr. Clin. Neurophysiol. 1994; 90:456–460. [PubMed: 7515789]

Pfurtscheller G, Lopes da Silva FH. Event-related EEG/MEG synchronization and desynchronization: basic principles. Clin. Neurophysiol. Off. J. Int. Fed. Clin. Neurophysiol. 1999; 110:1842–1857.

Poon C, Chin-Cottongim LG, Coombes SA, Corcos DM, Vaillancourt DE. Spatiotemporal dynamics of brain activity during the transition from visually guided to memory-guided force control. J. Neurophysiol. 2012; 108:1335–1348. [PubMed: 22696535]

Sauseng P, Klimesch W. What does phase information of oscillatory brain activity tell us about cognitive processes? Neurosci. Biobehav. Rev. 2008; 32:1001–1013. [PubMed: 18499256]

Schmidt RA, Zelaznik H, Hawkins B, Frank JS, Quinn JT. Motor-output variability: a theory for the accuracy of rapid motor acts. Psychol. Rev. 1979; 47:415–451. [PubMed: 504536]

Seidler RD, Bloomberg JJ, Stelmach GE. Context-dependent arm pointing adaptation. Behav. Brain Res. 2001; 119:155–166. [PubMed: 11165331]

Serrien DJ, Brown P. The integration of cortical and behavioural dynamics during initial learning of a motor task. Eur. J. Neurosci. 2003; 17:1098–1104. [PubMed: 12653986]

Shadmehr R, Smith MA, Krakauer JW. Error Correction, Sensory Prediction, and Adaptation in Motor Control. Annu. Rev. Neurosci. 2010; 33:89–108. [PubMed: 20367317]

Shattuck DW, Chiang M-C, Barysheva M, McMahon KL, de Zubicaray GI, Meredith M, Wright MJ, Toga AW, Thompson PM. Visualization tools for high angular resolution diffusion imaging. Med. Image Comput. Comput.-Assist. Interv. MICCAI Int. Conf. Med. Image Comput. Comput.-Assist. Interv. 2008; 11:298–305.

Sosnoff JJ, Newell KM. Intermittent visual information and the multiple time scales of visual motor control of continuous isometric force production. Percept. Psychophys. 2005; 67:335–344. [PubMed: 15971695]

Szurhaj W, Derambure P, Labyt E, Cassim F, Bourriez J-L, Isnard J, Guieu J-D, Mauguière F. Basic mechanisms of central rhythms reactivity to preparation and execution of a voluntary movement: a stereoelectroencephalographic study. Clin. Neurophysiol. Off. J. Int. Fed. Clin. Neurophysiol. 2003; 114:107–119.

Tan H, Jenkinson N, Brown P. Dynamic Neural Correlates of Motor Error Monitoring and Adaptation during Trial-to-Trial Learning. J. Neurosci. 2014; 34:5678–5688. [PubMed: 24741058]

Vaillancourt DE, Thulborn KR, Corcos DM. Neural basis for the processes that underlie visually guided and internally guided force control in humans. J. Neurophysiol. 2003; 90:3330–3340. [PubMed: 12840082]

Vukelić M, Bauer R, Naros G, Naros I, Braun C, Gharabaghi A. Lateralized alpha-band cortical networks regulate volitional modulation of beta-band sensorimotor oscillations. NeuroImage. 2014; 87:147–153. [PubMed: 24121086]

Woodworth RS. Accuracy of voluntary movement. Psychol. Rev. Monogr. 1899; (Suppl. 3) i-114.

Wróbel A, Ghazaryan A, Bekisz M, Bogdan W, Kamiński J. Two Streams of Attention-Dependent β Activity in the Striate Recipient Zone of Cat's Lateral Posterior-Pulvinar Complex. J. Neurosci. 2007; 27:2230–2240. [PubMed: 17329420]

Summary Statement

Our findings establish a link between sensorimotor oscillations in the context of online motor performance in common source space across subjects. Specifically, the extent and distinct role of medial parietal cortex to sensorimotor beta connectivity and local domain broadband activity combine in a time and frequency manner to assist ballistic movements. These findings can serve as a model to examine whether similar source space EEG dynamics exhibit different time-frequency changes in individuals with neurological disorders that cause movement errors.

Highlights

- Cortical activity and connectivity 1 were examined during upper limb movement
- Visual feedback gain led to better motor performance and increased muscle activity
- Increased theta-, alpha-, and beta-band desynchronization at high gain feedback
- Increased parietal-to-motor cortex connectivity in the beta-band at high gain feedback
- Visual gain did not affect motor-to-parietal cortex connectivity

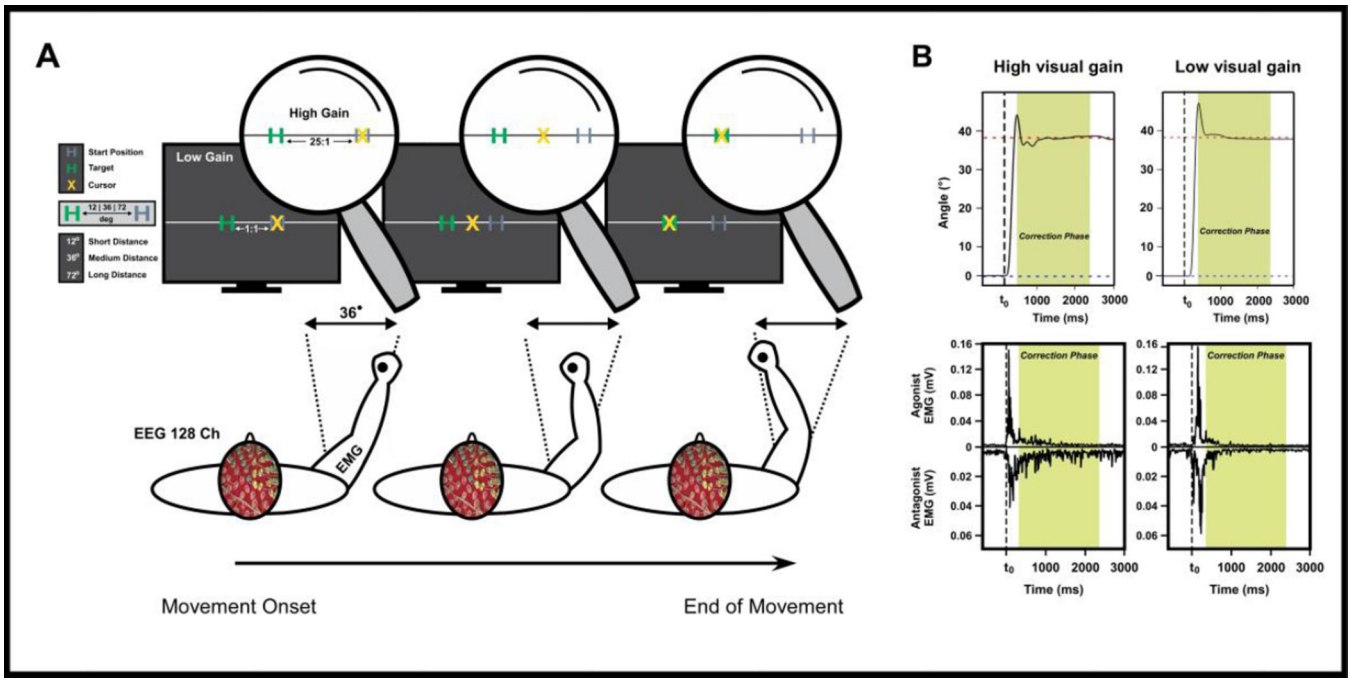

Figure 1. Experimental setup, and illustration of kinematic and neuromuscular data

Schematic representation of the desired body configuration (transverse plane) during various phases of the movement (A). We illustrate the visual feedback displayed on the monitor for the 36° angular distance condition. The gray H character on the monitor indicates the start position, the green H character indicates the target position, and the yellow X character indicates the angular position of the participant's arm. Section B shows angular position data, agonist, and antagonist EMG time series data for high and low visual gain conditions from one subject. The green shaded area indicates the post ballistic movement (PBM) phase.

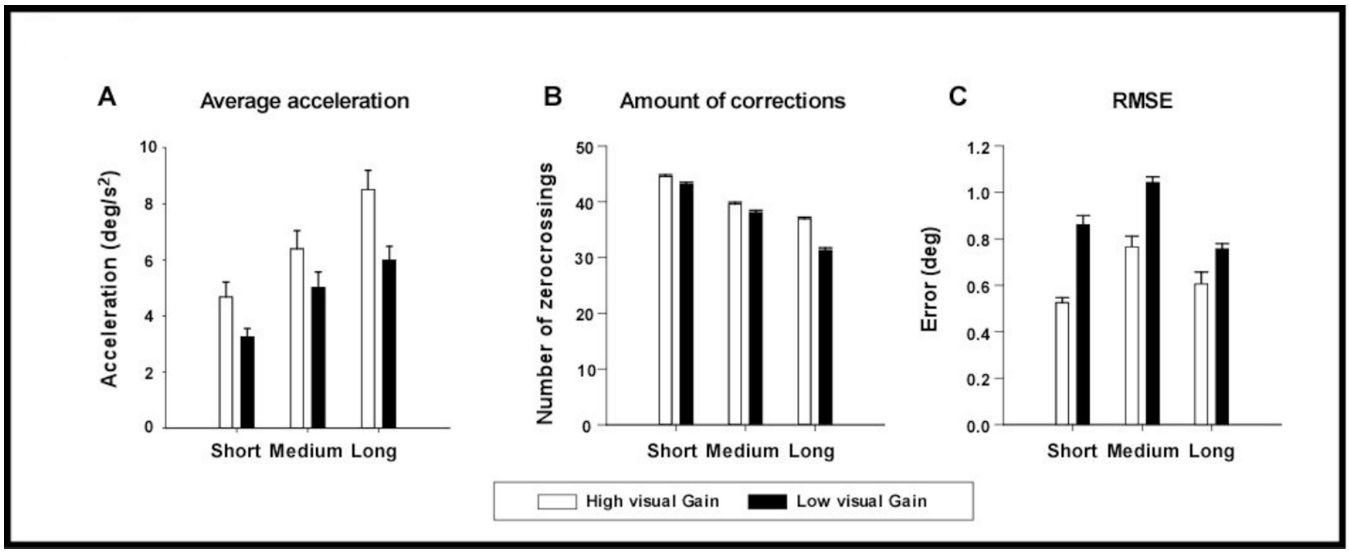

Figure 2. Gain effects on task performance

Gain effects during the PBM phase on task performance variables: average acceleration (A), number of zero-crossings (B), and RMSE (C) for short, medium and long distances. Error bars represent standard error (N=16).

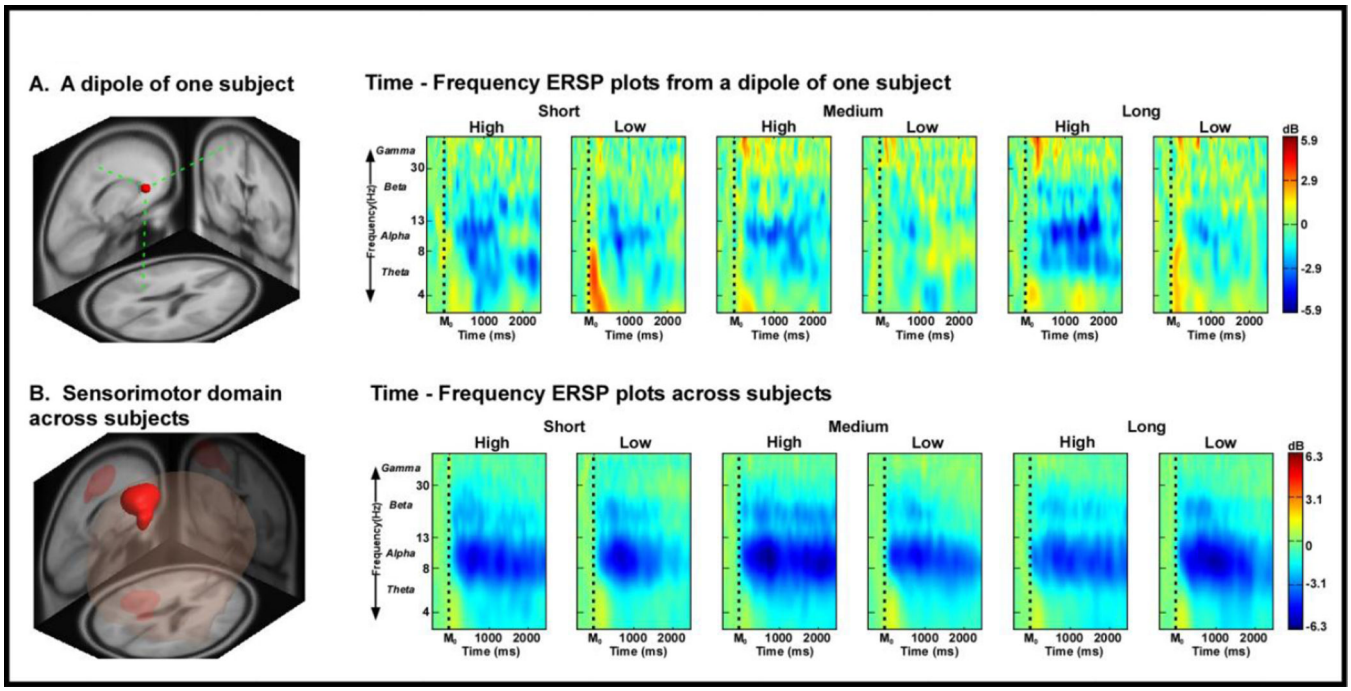

Figure 3. ERSP time-frequency plots within the sensorimotor domain

ERSP time-frequency plot from a dipole located in the sensorimotor area for one subject (A), and ERSP time-frequency plots for high and low visual gain conditions across all 16 subjects (B). The x-axis denotes time with M_0 representing movement onset. The logarithmic y-axis depicts frequencies from 3 to 50 with the major EEG bands, theta, alpha, beta, and gamma labeled. The ERSP plots are color coded based on decibel where positive values are warm colors and negative values are cool colors.

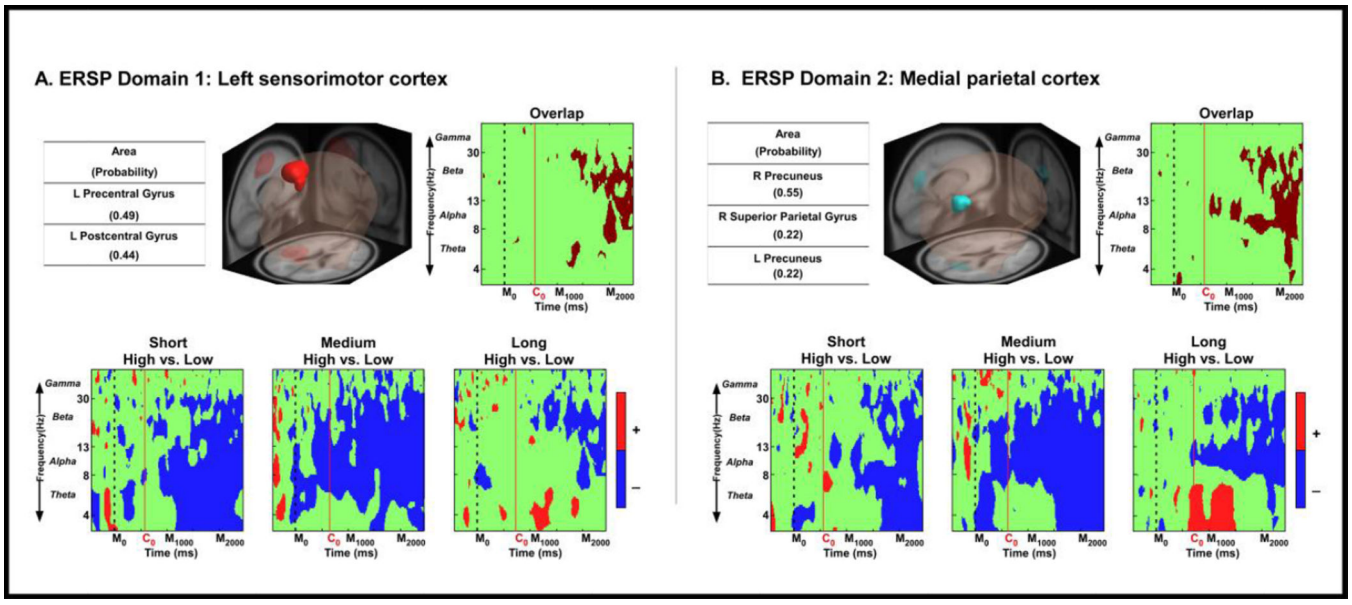

Figure 4. ERSP measure domains as revealed by MPA analysis and time-frequency contrast statistical plots

Section A shows domain 1 in the left motor area as revealed by the MPA analysis, whereas section B displays domain 2 in the medial parietal cortex. For each domain, the bottom panel depicts the ERSP time-frequency plots corresponding to the high gain vs. low gain comparison for each distance (i.e., short, medium, and long). The x-axis denotes time with M_0 representing movement onset, C_0 representing the average onset time of the PBM phase whereas M_{1000} represents 1000 ms after movement onset and M_{2000} represents 2000 ms after movement onset. The logarithmic y-axis depicts frequencies from 3 to 50 with the major EEG bands, theta, alpha, beta, and gamma labeled. The plots of the bottom panel are color scaled based on the statistical differences from the non-parametric test, where positive values are when high gain is more synchronization, and negative values are when high gain is more desynchronization. The green regions indicate non-significant areas. Also, for each domain, common time-frequency statistical results are displayed in the right upper panel labeled Overlap.

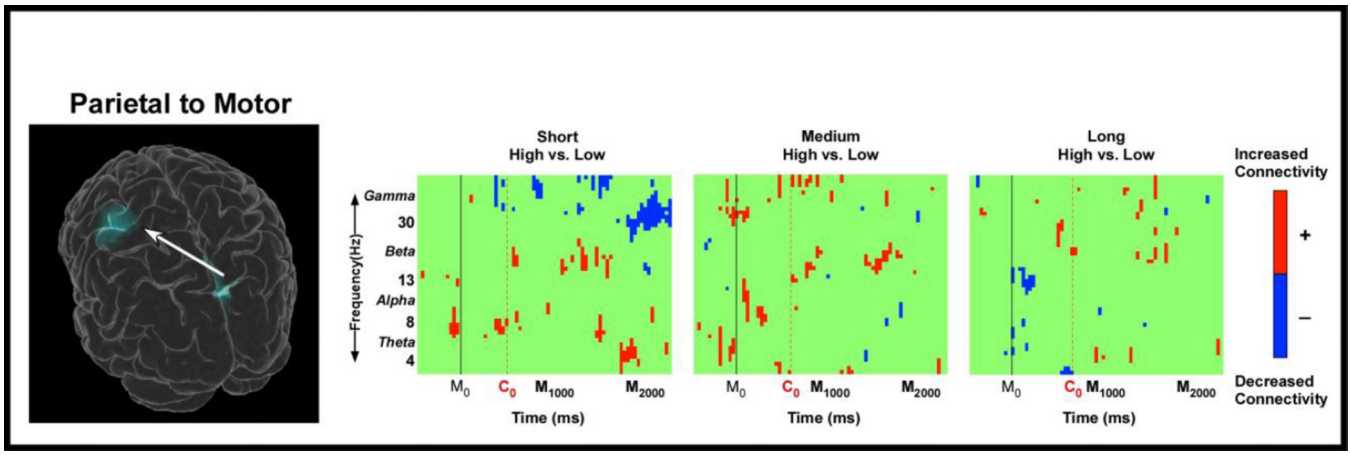

Figure 5. Spatial distribution of effective connectivity as measured by dDTF

The two ERSP domains for which effective connectivity was measured (left contralateral motor cortex and medial parietal cortex) and the directionality of the connectivity are displayed on the 3D glass brain. The adjacent plots illustrate the dDTF magnitude time-frequency statistical comparison between high and low visual gains across all distance conditions. Plots are color coded based on the significant FDR corrected dDTF values. Red color indicates increased connectivity from the parietal domain to the motor domain in the high gain condition compared to the low gain condition, whereas blue color indicates decreased connectivity from the parietal domain to the motor domain in the high gain condition compared to the low gain condition. Connectivity from the motor domain to the parietal domain was not significant. The x-axis denotes time with M_0 representing movement onset, C_0 representing the average onset time of the PBM phase whereas M_{1000} represents 1000 ms after movement onset and M_{2000} represents 2000 ms after movement onset. The y-axis depicts frequencies from 0 to 50 with the major EEG bands, theta, alpha, beta, and gamma labeled.

Table 1

Gain and distance effects on kinematic and EMG measures

Variables	Short		Medium		Long		Distance Effect		Gain Effect		Interaction	
	High Gain	Low Gain	High Gain	Low Gain	High Gain	Low Gain	F-value	*p*-value	F-value	*p*-value	F-value	*p*-value
Peak Displ	14.5 (0.4)	13.2 (0.3)	38.9 (0.5)	37.6 (0.5)	74.6 (0.5)	73.6 (0.4)	6023.116	<0.0001	11.574	0.0074	6.235	0.1085
Peak Vel	74.2 (5.5)	67.3 (6.3)	170.0 (12.0)	181.0 (17.6)	290.6 (23.9)	291.0 (23.8)	1045.048	<0.0001	0.863	0.4242	2.905	0.2108
Peak Accel	909.8 (111.9)	875.3 (130.8)	1566.8 (195.5)	1932.2 (334.8)	2191.2 (372.5)	2315.8 (393.7)	63.996	<0.0001	0.444	0.5521	2.022	0.3215
Peak Vel Time	271.5 (4.8)	273.8 (4.7)	284.6 (6.2)	277.7 (6.7)	298.0 (7.8)	294.7 (7.9)	20.79	<0.0001	1.638	0.2751	1.58	0.4174
Peak Accel Time	114.3 (2.7)	116.2 (2.5)	119.1 (4.1)	117.6 (3.5)	128.8 (4.4)	127.5 (3.9)	16.361	<0.0001	0.000	0.986	0.362	0.7492
Peak Decel Time	437.7 (7.1)	435.8 (6.8)	448.4 (9.4)	438.4 (9.7)	462.2 (11.5)	459.3 (11.6)	9.531	0.0083	2.145	0.2232	0.491	0.7152
Ave Accel − 1st sec PBM	4.68 (0.53)	3.25 (0.31)	6.39 (0.65)	5.02 (0.55)	8.50 (0.68)	5.99 (0.49)	58.792	<0.0001	25.399	0.0007	0.562	0.7152
RMSE-PBM Phase	0.53 (0.08)	0.86 (0.16)	0.77 (0.19)	1.04 (0.10)	0.61 (0.21)	0.76 (0.09)	2.504	0.1139	20.475	0.0015	0.245	0.7843
SD - PBM Phase	0.07 (0.005)	0.10 (0.01)	0.80 (0.01)	0.11 (0.01)	0.10 (0.01)	0.10 (0.01)	4.259	0.0294	7.116	0.0263	8.34	0.0198
Zero-crossing – PBM	44.5 (1.3)	43.2 (1.3)	39.6 (1.5)	38.1 (1.7)	36.9 (1.1)	31.3 (1.8)	34.74	<0.0001	16.472	0.0022	5.54	0.1085
Zero-crossing Start Time	583.5 (18.0)	629.8 (27.9)	639.5 (15.6)	635.9 (26.7)	691.9 (26.9)	731.6 (39.4)	34.74	<0.0001	16.472	0.0022	5.54	0.1085
Biceps EMG	7.6 (1.8)	4.9 (0.8)	10.5 (2.6)	9.0 (2.8)	11.3 (3.0)	8.5 (2.0)	6.093	0.0083	28.617	0.0007	0.486	0.7152
Brach EMG	6.9 (0.9)	6.0 (0.8)	9.1 (2.0)	7.9 (1.4)	10.3 (2.0)	9.0 (2.5)	9.596	0.0083	16.906	0.0022	0.815	0.6783
Tri-lat EMG	7.1 (1.1)	6.0 (0.9)	8.5 (1.8)	6.8 (1.4)	8.9 (2.1)	6.2 (1.3)	0.207	0.6538	25.885	0.0007	0.686	0.6783
Tri-long EMG	7.0 (1.2)	5.8 (0.7)	6.8 (1.0)	7.2 (1.3)	7.4 (1.3)	5.1 (0.8)	1.615	0.2311	9.285	0.0136	2.21	0.3181

Table legend: Accel, Acceleration; Ave, Average; Displ, Displacement; PBM , Post ballistic movement; RMSE, Root mean square error; Decel, Deceleration; Brach, Brachioradialis; Tri-lat, Triceps lateral; Tri-long, Triceps longitudinal, Values in cells under each condition represent mean values and values in parentheses are standard error values.